

This collage contains several distinct diagrams:

- Top Left:** An electrical circuit diagram featuring a DC voltage source (represented by a battery symbol), a resistor, and an inductor connected in series. A diamond-shaped component with '+' and '-' terminals is also part of the circuit.
- Top Center:** A diagram of a motor or actuator with a cylindrical body and mounting brackets. A curved arrow indicates its rotational motion.
- Top Right:** A schematic of a robotic arm with a grey base, yellow segments, and a black end effector holding a spherical object.
- Middle Left:** A diagram showing a yellow rectangular block on a blue horizontal track, connected to a grey base by a thin rod.
- Middle Right:** A diagram of a light fixture with three yellow light bulbs mounted on a black horizontal bar.
- Bottom Left:** A 3D perspective drawing of a mechanical assembly, possibly a valve or a connector, with a blue cylindrical component and white rectangular blocks.
- Bottom Right:** A diagram of a control system or interface, featuring a green horizontal bar, a red square button, and three red square buttons at the bottom.

Title: Adaptive Visual Servo Regulation Control for Camera-in-Hand Configuration with a Fixed-Camera Extension

Authors: Enver Tatlicioglu, Darren Dawson, and Bin Xian

Report Documentation Page				Form Approved OMB No. 0704-0188	
Public reporting burden for the collection of information is estimated to average 1 hour per response, including the time for reviewing instructions, searching existing data sources, gathering and maintaining the data needed, and completing and reviewing the collection of information. Send comments regarding this burden estimate or any other aspect of this collection of information, including suggestions for reducing this burden, to Washington Headquarters Services, Directorate for Information Operations and Reports, 1215 Jefferson Davis Highway, Suite 1204, Arlington VA 22202-4302. Respondents should be aware that notwithstanding any other provision of law, no person shall be subject to a penalty for failing to comply with a collection of information if it does not display a currently valid OMB control number.					
1. REPORT DATE 09 MAR 2007		2. REPORT TYPE		3. DATES COVERED 00-00-2007 to 00-00-2007	
4. TITLE AND SUBTITLE Adaptive Visual Servo Regulation Control for Camera-in-Hand Configuration with a Fixed-Camera Extension				5a. CONTRACT NUMBER	
				5b. GRANT NUMBER	
				5c. PROGRAM ELEMENT NUMBER	
6. AUTHOR(S)				5d. PROJECT NUMBER	
				5e. TASK NUMBER	
				5f. WORK UNIT NUMBER	
7. PERFORMING ORGANIZATION NAME(S) AND ADDRESS(ES) Clemson University ,College of Engineering and Science,109 Riggs Hall,Clemson,SC,29631-0901				8. PERFORMING ORGANIZATION REPORT NUMBER	
9. SPONSORING/MONITORING AGENCY NAME(S) AND ADDRESS(ES)				10. SPONSOR/MONITOR'S ACRONYM(S)	
				11. SPONSOR/MONITOR'S REPORT NUMBER(S)	
12. DISTRIBUTION/AVAILABILITY STATEMENT Approved for public release; distribution unlimited					
13. SUPPLEMENTARY NOTES The original document contains color images.					
14. ABSTRACT					
15. SUBJECT TERMS					
16. SECURITY CLASSIFICATION OF:			17. LIMITATION OF ABSTRACT	18. NUMBER OF PAGES 11	19a. NAME OF RESPONSIBLE PERSON
a. REPORT unclassified	b. ABSTRACT unclassified	c. THIS PAGE unclassified			

Adaptive Visual Servo Regulation Control for Camera-in-Hand Configuration with a Fixed-Camera Extension

Enver Tatlicioglu*, Darren M. Dawson, and Bin Xian

Abstract: In this paper, image-based regulation control of a robot manipulator with an uncalibrated vision system is discussed. To compensate for the unknown camera calibration parameters, a novel prediction error formulation is presented. To achieve the control objectives, a Lyapunov-based adaptive control strategy is employed. The control development for the camera-in-hand problem is presented in detail and a fixed-camera problem is included as an extension.

I. INTRODUCTION

The use of computer vision data to control the motion of a robot manipulator is commonly referred to as visual servo control. For single camera systems, the vision data may be acquired from the camera which is mounted at the end-effector of the robot manipulator (camera-in-hand) or the camera may be fixed in the workspace (fixed-camera) so that it can observe the motion of the end-effector of the robot manipulator. For both camera-in-hand and fixed-camera systems, the two dominant control architectures are image-based visual servo control and position-based visual servo control [1]. For image-based control schemes, the Jacobian matrix, which maps the image errors onto the joint space of the manipulator is commonly referred as the interaction matrix. The interaction matrix is a nonlinear function of the intrinsic and extrinsic camera calibration parameters. Hence, the performance of the controller depends on the accurate knowledge of the camera parameters [2]. However, camera calibration is tedious, difficult and costly [2], [3]. On the other hand, a control scheme with off-line identification of the camera calibration parameters is usually not robust to the change of parameters, disturbances, and unknown environments [4].

Beginning from the early 1990's, the focus of much of the research on visual servoing has moved to uncalibrated vision systems. Yoshimi and Allen [5] utilized the geometric effect of rotational invariance to estimate the interaction matrix. Hosoda and Asada [4] presented an extended least squares algorithm with exponential data weighting for estimating the

interaction matrix. In [6], Fakhry and Wilson presented modifications of the resolved acceleration controller for visual servoing. Jagersand et al. [7] proposed an adaptive visual servoing controller. In [7], a nonlinear least-squares optimization method using a trust region method and Broyden estimation is utilized. The method proposed in [7] is similar to the ones in [6] and [4]. Bishop and Spong [8] presented a sampled-data controller for uncalibrated monocular visual servo systems with an online calibration extension. In [9], Ruf et al. proposed an online calibration algorithm for position-based visual servo control. In [10] and [11], Papanikolopoulos et. al. proposed an algorithm based on online estimation of the relative distance of the target with respect to the camera. In [12], Malis proposed a visual servo controller which is robust to changes in the intrinsic camera calibration parameters. Piepmeier et al. [13] proposed a dynamic quasi-Newton method for visual servo control of uncalibrated robotic systems. In [13], where a recursive least squares algorithm is utilized to estimate the unknown interaction matrix. In [14], Lu et al. presented an online algorithm using the least square method to calculate the extrinsic orientation matrix. In [15], Hespanha et al. developed theoretical analysis for uncalibrated stereo systems. In [16], a visual servo controller is presented for end-effector regulation tasks in the presence of uncertain camera calibration parameters. In [17], Kelly et al. suggested two controllers based on the transpose Jacobian control philosophy. However, the first controller requires the depth information for all the feature points, and the second controller depends on the approximate Jacobian method which utilizes the best available information on the depth and the camera calibration parameters. Recently, Liu et al. [2] presented adaptive controllers for uncalibrated fixed-camera systems. The first controller tracks only one feature point and the second controller can track multiple feature points. However, with a six degree-of-freedom robot manipulator, the proposed controller can track at most three feature points. This constitutes a problem based on the well-known fact that four coplanar feature points on an object are needed to determine its posture from their projection in the image plane. Similar to [2], the development in [18] is also for tracking control of one feature point.

In this paper, image-based regulation control of a robot manipulator with an uncalibrated vision system (i.e., the intrinsic and extrinsic camera parameters are unknown) is addressed. To compensate for the unknown camera calibration parameters, a prediction error formulation is presented. For all the feature points, the interaction matrix and the depth are both linearly parameterized, which is then followed by

This work is supported in part by a DOC Grant, an ARO Automotive Center Grant, a DOE Contract, a Honda Corporation Grant, and a DARPA Contract.

* To whom all the correspondence should be addressed.

E. Tatlicioglu is with the Department of Electrical & Computer Engineering, Clemson University, Clemson, SC 29634-0915 (phone/fax: 864-656-7218; e-mail: etatlic@clemson.edu).

D. M. Dawson is with the Department of Electrical & Computer Engineering, Clemson University, Clemson, SC 29634-0915 (darren.dawson@ces.clemson.edu).

B. Xian is with School of Electrical Engineering and Automation, Tian Jin University, Tian Jin 300072, P.R.China (e-mail: xbin@tju.edu.cn).

a novel prediction error formulation to design the nonlinear estimation law. The novelty of this formulation over the past research is its unique method to linearly parameterize the interaction matrix and the depth simultaneously. To develop the error system, the image error signals for four feature points are combined to form the final error signal which is followed by the Lyapunov-based stability analysis. The novelty of this analysis is the design of the Lyapunov function which incorporates the depth informations for all feature points. Satisfaction of persistent excitation (PE) conditions allows the image and the estimation error signals to be driven to zero. The control development for the camera-in-hand problem is presented in detail and a fixed-camera problem is included as an extension.

II. ADAPTIVE CONTROL FOR CAMERA-IN-HAND CONFIGURATION

A. Geometric Model

To make the subsequent development more tractable, four coplanar target points located on a static object, denoted by $O_i \forall i = 1, \dots, 4$ are considered. In order to develop a geometric relationship between the fixed object and the moving camera, an inertial coordinate frame, denoted by \mathcal{I} , attached to the object, an orthogonal coordinate frame, denoted by \mathcal{F} , whose origin coincides with the optical center of the moving camera, an inertial coordinate frame, denoted by \mathcal{W} , attached to the base frame of the robot manipulator, and an orthogonal coordinate frame, denoted by \mathcal{E} , attached to the end-effector of the robot manipulator are defined (see Figure 1). Let the 3D coordinates of the i^{th} feature point on the object be denoted as the constant $x_{pi} \in \mathbb{R}^3$ relative to the base frame \mathcal{W} , and $\bar{m}_i(t) \in \mathbb{R}^3$ relative to \mathcal{F} , which is defined as follows

$$\bar{m}_i \triangleq [x_i \ y_i \ z_i]^T. \quad (1)$$

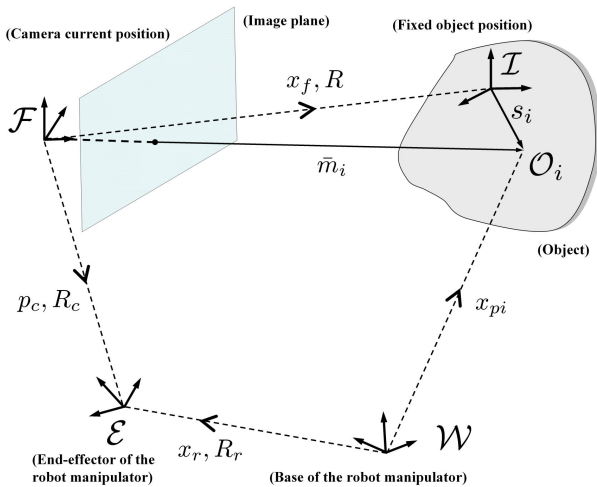


Fig. 1. Geometric relationships between the fixed object, robot manipulator, and the camera attached to its end-effector.

In the subsequent development, it is assumed that the object is always in the field of view (fov) of the camera, hence the distances from the origin of \mathcal{I} to all feature points remain positive (i.e., $z_i(t) > \varepsilon$ where $\varepsilon \in \mathbb{R}$ is an arbitrarily small positive constant) and bounded. To relate the coordinate systems, let $R(t) \in SO(3)$ and $x_f(t) \in \mathbb{R}^3$ denote the rotation matrix and the translation vector respectively, between \mathcal{F} and \mathcal{I} . Let $m_i(t) \in \mathbb{R}^3$ denote the normalized Euclidian coordinates for the i^{th} feature point, which is defined as follows

$$m_i \triangleq \frac{1}{z_i} \bar{m}_i. \quad (2)$$

In the image captured by the camera, each of these feature points have projected pixel coordinates expressed relative to \mathcal{I} , denoted by $p_i(t) \in \mathbb{R}^2$, defined as follows

$$p_i \triangleq [u_i \ v_i]^T \quad (3)$$

where $u_i(t), v_i(t) \in \mathbb{R}$. The projected pixel coordinates of the feature points are related to the normalized Euclidian coordinates by the pin-hole model of [19] such that

$$p_i \triangleq \bar{A} m_i \quad (4)$$

where $\bar{A} \in \mathbb{R}^{2 \times 3}$ is the unknown truncated camera calibration matrix [20] which is assumed to be of the following form

$$\bar{A} \triangleq \begin{bmatrix} f k_u & f k_u \cot \phi & u_0 \\ 0 & \frac{f k_v}{\sin \phi} & v_0 \end{bmatrix} \quad (5)$$

where $k_u, k_v \in \mathbb{R}$ denote camera scaling factors, $u_0, v_0 \in \mathbb{R}$ represent the pixel coordinates of the principal point, $\phi \in \mathbb{R}$ is the angle between the camera axes, and $f \in \mathbb{R}$ is the camera focal length.

B. Open-Loop Error System

To facilitate the open-loop error system development, image error for the i^{th} feature point, denoted by $e_i(t) \in \mathbb{R}^2$, is defined as follows

$$e_i \triangleq p_i - p_{di} \quad (6)$$

where $p_{di} \in \mathbb{R}^2$ is the constant desired image coordinates for the i^{th} feature point. The dynamics of the image error is found as follows

$$\dot{e}_i = \dot{p}_i \quad (7)$$

$$= \frac{1}{z_i} \bar{A}_{ei} \dot{\bar{m}}_i \quad (8)$$

where $\bar{A}_{ei}(t) \in \mathbb{R}^{2 \times 3}$ is a function of camera intrinsic calibration parameters and image coordinates of the i^{th} feature point as shown below

$$\bar{A}_{ei} \triangleq \bar{A} - \begin{bmatrix} 0 & 0 & u_i \\ 0 & 0 & v_i \end{bmatrix} \quad (9)$$

and from Figure 1, $\dot{\bar{m}}_i(t)$ can be found to be of the following form

$$\dot{\bar{m}}_i = R_c \begin{bmatrix} -R_r & S[R_r(x_{pi} - x_r)] \end{bmatrix} J_r \dot{q} \quad (10)$$

where the forward kinematics of the robot manipulator was utilized [21]. In (10), $R_c \in SO(3)$ is the camera extrinsic calibration matrix, $R_r(t) \in SO(3)$ is the orientation matrix of the end-effector of the robot manipulator, $J_r(q) \in \mathbb{R}^{6 \times 6}$ is the Jacobian matrix of the robot manipulator, $x_r(t) \in \mathbb{R}^3$ is the end-effector position of the robot manipulator relative to \mathcal{W} , $q(t) \in \mathbb{R}^6$ represents the joint positions of the robot manipulator, and $S(\cdot) \in \mathbb{R}^{3 \times 3}$ is the skew-symmetric matrix form of its argument defined as follows

$$S(\xi) \triangleq \begin{bmatrix} 0 & -\xi_3 & \xi_2 \\ \xi_3 & 0 & -\xi_1 \\ -\xi_2 & \xi_1 & 0 \end{bmatrix}, \forall \xi = \begin{bmatrix} \xi_1 \\ \xi_2 \\ \xi_3 \end{bmatrix}. \quad (11)$$

The joint velocity vector $\dot{q}(t) \in \mathbb{R}^6$ is assumed to be the kinematic control input such that

$$u \triangleq \dot{q}. \quad (12)$$

After utilizing (10) and (12), the dynamics for the image error of (8) can be rewritten as follows

$$z_i \dot{e}_i = \bar{A}_{ei} R_c \begin{bmatrix} -R_r & S[R_r(x_{pi} - x_r)] \end{bmatrix} J_r u. \quad (13)$$

Remark 1: In [22], it was shown that four non-collinear object feature points are sufficient to determine the end-effector frame pose with respect to the base frame. Based on this fact, the analysis in this paper will be based on regulation of four feature points.

Remark 2: In the subsequent analysis, it is assumed that the end-effector position of the robot manipulator $x_r(t)$, the orientation matrix of the end-effector of the robot manipulator $R_r(t)$, and the Jacobian matrix of the robot manipulator $J_r(q)$ are known, and the camera intrinsic and extrinsic calibration matrices (i.e., R_c and \bar{A}) are constant and unknown.

Remark 3: In the subsequent analysis, it is assumed that the joint positions of the robot manipulator are bounded (i.e., $q(t) \in \mathcal{L}_\infty$) provided that the projected pixel coordinates of all feature points are bounded (i.e., $p_i(t) \in \mathcal{L}_\infty \forall i = 1, \dots, 4$).

Remark 4: In the subsequent analysis, it is assumed that the orientation matrix of the end-effector of the robot manipulator $R_r(t)$ and the Jacobian matrix of the robot manipulator $J_r(q)$ are bounded signals provided that the joint positions of the robot manipulator are bounded.

After utilizing (1) and (10), the dynamics of $z_i(t)$ are obtained as follows

$$\dot{z}_i = r_{c3}^T \begin{bmatrix} -R_r & S[R_r(x_{pi} - x_r)] \end{bmatrix} J_r u \quad (14)$$

where $r_{c3}^T \in \mathbb{R}^{1 \times 3}$ is the third row vector of the extrinsic camera calibration matrix. To facilitate the subsequent analysis a diagonal matrix, denoted by $Z(t) \in \mathbb{R}^{8 \times 8}$, with its entries being $z_i(t) \forall i = 1, \dots, 4$, and a combined error signal $e(t) \in \mathbb{R}^8$ are defined as follows

$$Z \triangleq \text{diag} \{z_1, z_1, z_2, z_2, z_3, z_3, z_4, z_4\} \quad (15)$$

$$e \triangleq \begin{bmatrix} e_1^T & e_2^T & e_3^T & e_4^T \end{bmatrix}^T. \quad (16)$$

We can see from (15) and (16) that the product $Z(t)e(t)$ is equal to the following expression

$$Ze = \begin{bmatrix} z_1 e_1^T & z_2 e_2^T & z_3 e_3^T & z_4 e_4^T \end{bmatrix}^T. \quad (17)$$

After utilizing (13), (15) and (16), the following expression can be obtained for $Z(t)\dot{e}(t)$

$$Z\dot{e} = \begin{bmatrix} z_1 \dot{e}_1^T & z_2 \dot{e}_2^T & z_3 \dot{e}_3^T & z_4 \dot{e}_4^T \end{bmatrix}^T \quad (18)$$

$$= B_1 J_r u. \quad (19)$$

where $B_1(t) \in \mathbb{R}^{8 \times 6}$ is defined in Appendix I. After adding and subtracting the term $\frac{1}{2}\dot{Z}(t)e(t)$ to the right-hand-side of (19), the following expression can be obtained

$$Z\dot{e} = -\frac{1}{2}\dot{Z}(t)e(t) + \Pi u \quad (20)$$

where $\Pi(t) \in \mathbb{R}^{8 \times 6}$ is defined in Appendix I. Since, the auxiliary matrix $\Pi(t)$ has unknown constant parameters, the product $\Pi(t)u(t)$ can be linearly parameterized as follows

$$\Pi u = W_3 \Theta \quad (21)$$

where $W_3(t) \in \mathbb{R}^{8 \times p}$ is a known regressor matrix, and $\Theta \in \mathbb{R}^p$ is an unknown constant parameter vector¹. The estimation form of (21) can be defined as follows

$$\hat{\Pi} u = W_3 \hat{\Theta} \quad (22)$$

where $\hat{\Pi}(t) \in \mathbb{R}^{8 \times 6}$ is the estimate of $\Pi(t)$, and $\hat{\Theta}(t) \in \mathbb{R}^p$ is the yet to be defined dynamic estimate of Θ . After adding and subtracting $\hat{\Pi}(t)u(t)$ to the right-hand-side of (20), the following open-loop error system is obtained

$$Z\dot{e} = -\frac{1}{2}\dot{Z}(t)e(t) + \hat{\Pi}u + W_3 \tilde{\Theta} \quad (23)$$

where the following expression was utilized

$$\tilde{\Pi} u = W_3 \tilde{\Theta} \quad (24)$$

with $\tilde{\Pi}(t) \in \mathbb{R}^{8 \times 6}$ being defined as follows

$$\tilde{\Pi} \triangleq \Pi - \hat{\Pi} \quad (25)$$

and $\tilde{\Theta}(t) \in \mathbb{R}^p$ is the estimation error defined as follows

$$\tilde{\Theta} \triangleq \Theta - \hat{\Theta}. \quad (26)$$

C. Closed-Loop Error System

Based on the subsequent stability analysis, the control input $u(t)$ is designed as follows

$$u \triangleq -k\hat{\Pi}^T e \quad (27)$$

where $k \in \mathbb{R}$ is a positive constant control gain. After substituting (27) into the open-loop error system in (23), the following closed-loop error system is obtained

$$Z\dot{e} = -\frac{1}{2}\dot{Z}(t)e(t) - k\hat{\Pi}\hat{\Pi}^T e + W_3 \tilde{\Theta}. \quad (28)$$

¹The reader is referred to [23] for the derivation of $W_3(t)$ and Θ .

D. Prediction Error Formulation

In this section, a prediction error formulation for the unknown parameters will be introduced. From Figure 1, $\bar{m}_i(t)$ can be written as follows²

$$\bar{m}_i = R_c [R_r^T (x_{pi} - x_r) + p_c] \quad (29)$$

where $p_c \in \mathbb{R}^3$ is the position of the origin of frame \mathcal{F} with respect to frame \mathcal{W} expressed in frame \mathcal{F} . After utilizing (1), (2), and (4), the pixel coordinates for the i^{th} feature point can be written as follows

$$p_i = \frac{1}{z_i} \bar{A} R_c [R_r^T (x_{pi} - x_r) + p_c] \quad (30)$$

where the corresponding depth can be written as follows

$$z_i = r_{c3}^T [R_r^T (x_{pi} - x_r) + p_c]. \quad (31)$$

where $r_{c3}^T \in \mathbb{R}^3$ is the last row of R_c . It should be noted that, in (30) and (31), \bar{A} , R_c , x_{pi} , p_c are unknown constant parameters, and $x_r(t)$, $R_r(t)$ are measurable signals (see Remark 2). Based on these facts, $p_i(t)$ can be linearly parameterized as follows

$$p_i = \frac{W_1 \Theta_{1i}}{W_2 \Theta_{2i}} \quad (32)$$

where the following linear parameterization of $z_i(t)$ was utilized

$$z_i = W_2 \Theta_{2i}. \quad (33)$$

We note that $z_i(t)$ are assumed to satisfy the following inequalities

$$\rho_i(\cdot) \geq z_i(t) = W_2(t) \Theta_{2i} \geq \varepsilon_i > 0 \quad (34)$$

where $\rho_i(m_i) \in \mathbb{R} \forall i$ are positive functions and $\varepsilon_i \in \mathbb{R} \forall i$ are positive constants. In (32) and (33), $W_1(t) \in \mathbb{R}^{2 \times r_1}$, $W_2(t) \in \mathbb{R}^{1 \times r_2}$ are measurable regression matrices, and $\Theta_{1i} \in \mathbb{R}^{r_1}$, $\Theta_{2i} \in \mathbb{R}^{r_2}$ are unknown constant parameter vectors³. After multiplying both sides of (32) with the term $W_2(t) \Theta_{2i}$ the following expression can be obtained

$$p_i W_2 \Theta_{2i} = W_1 \Theta_{1i}. \quad (35)$$

The estimation forms of (32) and (35) can be defined as follows

$$\hat{p}_i = \frac{W_1 \hat{\Theta}_{1i}}{W_2 \hat{\Theta}_{2i}} \quad (36)$$

$$\hat{p}_i W_2 \hat{\Theta}_{2i} = W_1 \hat{\Theta}_{1i} \quad (37)$$

where $\hat{\Theta}_{1i}(t) \in \mathbb{R}^{r_1}$ and $\hat{\Theta}_{2i}(t) \in \mathbb{R}^{r_2}$ are the estimates for Θ_{1i} and Θ_{2i} , respectively⁴. Subtracting (37) from (35)

²For the derivation of the expression for \bar{m}_i the reader is referred to Appendix VII.

³The reader is referred to [23] for the derivation of $W_1(t)$, $W_2(t)$, Θ_{1i} , and Θ_{2i} , $\forall i = 1, \dots, 4$.

⁴In the subsequent analysis, a projection algorithm will be utilized to make sure that $W_2(t) \hat{\Theta}_{2i}(t)$ is always greater than some arbitrarily small positive constant.

and adding and subtracting the term $\hat{p}_i(t) W_2(t) \Theta_{2i}$ to the right-hand-side results in the following expression

$$\tilde{p}_i = \frac{1}{W_2 \Theta_{2i}} \bar{W}_i [\tilde{\Theta}_{1i}^T \quad \tilde{\Theta}_{2i}^T]^T \quad (38)$$

where $\bar{W}_i(\hat{p}_i(t), t) \triangleq [W_1 \quad -\hat{p}_i W_2] \in \mathbb{R}^{2 \times (r_1 + r_2)}$ is a measurable signal, $\tilde{\Theta}_{ji}(t) \in \mathbb{R}^{r_j}$ is the estimation error defined as follows

$$\tilde{\Theta}_{ji} \triangleq \Theta_{ji} - \hat{\Theta}_{ji} \quad \forall j = 1, 2, \quad \forall i = 1, \dots, 4 \quad (39)$$

and the prediction error for the i^{th} feature point $\tilde{p}_i(t) \in \mathbb{R}^2$ is defined as follows

$$\tilde{p}_i \triangleq p_i - \hat{p}_i. \quad (40)$$

The combination of the pixel coordinates for all the feature points, denoted by $p(t) \in \mathbb{R}^8$, is defined as follows

$$p \triangleq [p_1^T \quad p_2^T \quad p_3^T \quad p_4^T]^T. \quad (41)$$

The prediction error $\tilde{p}(t) \in \mathbb{R}^8$ is defined as follows

$$\tilde{p} \triangleq p - \hat{p} \quad (42)$$

where $\hat{p}(t) \in \mathbb{R}^8$ is the estimation of $p(t)$. Based on (38) the prediction error $\tilde{p}(t)$ can be written as follows

$$\tilde{p} = F_1 \bar{W} \tilde{\Theta} \quad (43)$$

where $F_1(\cdot) \in \mathbb{R}^{8 \times 8}$ is an auxiliary matrix defined in Appendix I, and $\bar{W}(\cdot) \in \mathbb{R}^{8 \times p}$ is a measurable signal, $\Theta \in \mathbb{R}^p$ is the combination of the unknown constants, $\hat{\Theta}(t) \in \mathbb{R}^p$ is the estimation of Θ , and $\tilde{\Theta}(t) \in \mathbb{R}^p$ is the estimation error.

Remark 5: It should be noted that, when obtaining (43) from (38), there were common unknown constants for different feature points. As a result of this fact, an unknown vector Θ with the exact same size as in (26) is obtained.

Based on the subsequent stability analysis, the estimation law $\hat{\Theta}(t)$ is designed as follows

$$\dot{\hat{\Theta}} \triangleq \text{Proj} \{ \alpha \Gamma \bar{W}^T \tilde{p} + \Gamma W_3^T e \} \quad (44)$$

where $\text{Proj}\{\cdot\}$ is defined in Appendix VI, and $\alpha(t) \in \mathbb{R}$ is a positive scalar function defined as follows

$$\alpha \triangleq 1 + \frac{1}{\bar{\varepsilon}} \bar{\rho}(\cdot) \quad (45)$$

where $\bar{\rho}(\cdot) \in \mathbb{R}$ is a positive function defined as follows

$$\bar{\rho}(\cdot) \triangleq \max_i \{ \rho_i^2(\cdot) \} \quad (46)$$

and $\bar{\varepsilon} \in \mathbb{R}$ is a positive constant defined as follows

$$\bar{\varepsilon} \triangleq \min_i \{ \varepsilon_i \}. \quad (47)$$

In (44), $\Gamma(t) \in \mathbb{R}^{p \times p}$ is a least-squares estimation gain matrix designed as follows

$$\frac{d}{dt} (\Gamma^{-1}) \triangleq 2 \bar{W}^T \bar{W}. \quad (48)$$

Remark 6: It should be noted that if $\Gamma^{-1}(t_0)$ is selected to be positive definite and symmetric then $\Gamma(t_0)$ is also positive

definite and symmetric. Therefore it follows that both $\Gamma^{-1}(t)$ and $\Gamma(t)$ are positive definite and symmetric. From (48), the following expression can be obtained

$$\dot{\Gamma} = -2\Gamma\bar{W}^T\bar{W}\Gamma. \quad (49)$$

From (49), it is clear that $\dot{\Gamma}(t)$ is negative semidefinite; therefore, $\Gamma(t)$ is always constant or decreasing, and hence, it follows that $\Gamma(t)$ is bounded (for more details, the reader is referred to [24] and [25]).

E. Stability Analysis

Theorem 1: The control law defined in (27) and the update law defined in (44) ensure that $\|e(t)\|, \|\hat{\Theta}(t)\| \rightarrow 0$ as $t \rightarrow +\infty$ provided that the following persistent excitation conditions [26] hold

$$\gamma_1 I_8 \leq \int_{t_0}^{t_0+T} \hat{\Pi}(\tau) \hat{\Pi}^T(\tau) d\tau \leq \gamma_2 I_8 \quad (50)$$

$$\gamma_3 I_p \leq \int_{t_0}^{t_0+T} \bar{W}^T(\tau) \bar{W}(\tau) d\tau \leq \gamma_4 I_p \quad (51)$$

where $\gamma_i \in \mathbb{R} \forall i = 1, \dots, 4$ are positive constants, $I_8 \in \mathbb{R}^{8 \times 8}$ and $I_p \in \mathbb{R}^{p \times p}$ are identity matrices.

Proof: See Appendix II.

F. Conclusion

The image-based regulation control problem of a robot manipulator with an uncalibrated vision system was addressed. The depth information which is in the denominator, and the rest of the interaction matrix were simultaneously linearly parameterized for the first feature point. After utilizing a novel prediction error formulation the estimation law was designed. To avoid the singularity issue which might be caused by the depth signal appearing in the denominator, a parameter projection algorithm was utilized. Lyapunov-based analysis techniques were utilized to achieve the control objectives. The Lyapunov function was designed to embody the depth information of all feature points. This design of the Lyapunov function allowed us to have a depth-free stability analysis. Upon satisfaction of persistent excitation (PE) conditions, it was proven that both the image and the estimation error signals are driven to zero. As an extension, a fixed-camera configuration was presented.

REFERENCES

- [1] F. Chaumette and S. Hutchinson, "Visual servo control, part i: Basic approaches," *IEEE Robotics and Automation Magazine*, vol. 13, no. 4, pp. 82–90, December 2006.
- [2] Y. H. Liu, H. Wang, C. Wang, and K. K. Lam, "Uncalibrated visual servoing of robots using a depth-independent interaction matrix," *IEEE Tr. Robotics*, vol. 22, no. 4, pp. 804–817, August 2006.
- [3] Y. Shen, G. Xiang, Y. H. Liu, and K. Li, "Uncalibrated visual servoing of planar robots," in *Proc. IEEE Int. Conf. Robot. Autom.*, Washington, DC, 2002, pp. 580–585.
- [4] K. Hosada and M. Asada, "Versatile visual servoing without knowledge of true jacobian," in *Proc. IEEE/RSJ Int. Conf. Intell. Robots Syst.*, Munich, Germany, 1994, pp. 186–191.
- [5] B. H. Yoshimi and P. K. Allen, "Active, uncalibrated visual servoing," in *Proc. IEEE Int. Conf. Robot. Autom.*, San Diego, CA, 1994, pp. 156–161.
- [6] H. H. Fakhry and W. J. Wilson, "Modified resolved acceleration controller for position-based visual servoing," *Mathematical and computer modelling*, vol. 24, no. 5-6, pp. 1–9, 1996.
- [7] M. Jagersand, O. Fuentes, and R. Nelson, "Experimental evaluation of uncalibrated visual servoing for precision manipulation," in *Proc. IEEE Int. Conf. Robot. Autom.*, Albuquerque, NM, 1997, pp. 2874–2880.
- [8] B. E. Bishop and M. W. Spong, "Toward uncalibrated monocular visual servo," in *Proc. IEEE Int. Conf. Robot. Autom.*, Leuven, Belgium, 1998, pp. 2664–2669.
- [9] A. Ruf, M. Tonko, R. Horaud, and H.-H. Nagel, "Visual tracking of an end-effector by adaptive kinematic prediction," in *Proc. IEEE Int. Conf. Robot. Autom.*, Grenoble, France, 1997, pp. 893–898.
- [10] N. P. Papanikolopoulos and P. K. Khosla, "Adaptive robotic visual tracking: Theory and experiments," *IEEE Trans. Autom. Control*, vol. 38, no. 3, pp. 429–445, 1993.
- [11] N. P. Papanikolopoulos, B. J. Nelson, and P. K. Khosla, "Six degree-of-freedom hand/eye visual tracking with uncertain parameters," *IEEE Trans. Robot. Autom.*, vol. 11, no. 5, pp. 725–732, 1995.
- [12] E. Malis, "Visual servoing invariant to changes in camera-intrinsic parameters," *IEEE Trans. Robot. Autom.*, vol. 20, no. 1, pp. 72–81, February 2004.
- [13] J. A. Piepmeyer, G. V. McMurray, and H. Lipkin, "Uncalibrated dynamic visual servoing," *IEEE Trans. Robot. Autom.*, vol. 20, no. 1, pp. 143–147, 2004.
- [14] C.-P. Lu, E. Mjolsness, and G. D. Hager, "Online computation of exterior orientation with application to hand-eye calibration," *Mathematical and computer modelling*, vol. 24, no. 5-6, pp. 121–143, 1996.
- [15] J. Hespanha, Z. Dodds, G. D. Hager, and A. S. Morse, "What can be done with an uncalibrated stereo system," in *Proc. IEEE Int. Conf. Robot. Autom.*, Leuven, Belgium, 1998, pp. 1366–1372.
- [16] S. C. Solanki, W. E. Dixon, C. D. Crane, and S. Gupta, "Uncalibrated visual servo control of robot manipulators with uncertain kinematics," in *Proc. IEEE Int. Conf. Decision and Control*, San Diego, CA, 2006, pp. 3855–3860.
- [17] R. Kelly, E. Bugarin, I. Cervantes, and J. Alvarez-Ramirez, "Monocular direct visual servoing for regulation of manipulators moving in the 3d cartesian space," in *Proc. IEEE Int. Conf. Decision and Control*, San Diego, CA, 2006, pp. 1782–1787.
- [18] H. Wang and Y.-H. Liu, "Uncalibrated visual tracking control without visual velocity," in *Proc. IEEE Int. Conf. Robot. Autom.*, Orlando, FL, 2006, pp. 2738–2743.
- [19] O. Faugeras, *Three-Dimensional Computer Vision*. Cambridge, MA: MIT Press, 1993.
- [20] E. Malis and F. Chaumette, "2 1/2 d visual servoing with respect to unknown objects through a new estimation scheme of camera displacement," *International Journal of Computer Vision*, vol. 37, no. 1, pp. 79–97, 2000.
- [21] M. W. Spong and M. Vidyasagar, *Robot Dynamics and Control*. New York, NY: John Wiley and Sons, 1989.
- [22] J. Yuan, "A general photogrammetric method for determining object position and orientation," *IEEE Trans. Robot. Autom.*, vol. 5, no. 2, pp. 129–142, 1989.
- [23] E. Tatlicioglu, D. M. Dawson, and B. Xian, "Derivation of the regression matrices and the unknown coefficients for adaptive visual servo regulation control for camera-in-hand configuration with a fixed-camera extension," Clemson University CRB, Tech. Rep. CU/CRB/4/9/07/1, Apr. 2007. [Online]. Available: <http://www.ces.clemson.edu/ece/crb/publicn/tr.htm>
- [24] M. Krstic, I. Kanellakopoulos, and P. Kokotovic, *Nonlinear and Adaptive Control Design*. New York, NY: John Wiley and Sons, 1995.
- [25] M. de Queiroz, D. Dawson, S. Nagarkatti, and F. Zhang, *Lyapunov-Based Control of Mechanical Systems*. Boston, MA: Birkhauser, 1999.
- [26] J. J. E. Slotine and W. Li, *Applied Nonlinear Control*. Englewood Cliffs, NJ: Prentice Hall, 1991.
- [27] W. E. Dixon, A. Behal, D. M. Dawson, and S. Nagarkatti, *Nonlinear Control of Engineering Systems: A Lyapunov-Based Approach*. Boston, MA: Birkhauser, 2003.
- [28] H. K. Khalil, *Nonlinear Systems, 3rd Edition*. New York, NY: Prentice Hall, 2002.
- [29] V. K. Chitrakaran, D. M. Dawson, J. Chen, and W. E. Dixon, "Euclidean position estimation of features on a moving object using

APPENDIX I AUXILIARY DEFINITIONS

The auxiliary matrix $B_1(t)$, introduced in (19), is defined as follows

$$B_1 \triangleq \begin{bmatrix} \bar{A}_{e1} R_c & -R_r & S[R_r(x_{p1} - x_r)] \\ \bar{A}_{e2} R_c & -R_r & S[R_r(x_{p2} - x_r)] \\ \bar{A}_{e3} R_c & -R_r & S[R_r(x_{p3} - x_r)] \\ \bar{A}_{e4} R_c & -R_r & S[R_r(x_{p4} - x_r)] \end{bmatrix}. \quad (52)$$

After utilizing (16) and the time derivative of (15), the product $\dot{Z}(t)e(t)$ can be written as follows

$$\dot{Z}e = E_1 \frac{d}{dt} \begin{bmatrix} z_1 & z_1 & z_2 & z_2 & z_3 & z_3 & z_4 & z_4 \end{bmatrix}^T \quad (53)$$

where the diagonal matrix $E_1(t) \in \mathbb{R}^{8 \times 8}$ is defined as follows

$$E_1 \triangleq \text{diag} \{e_{11}, e_{12}, e_{21}, e_{22}, e_{31}, e_{32}, e_{41}, e_{42}\} \quad (54)$$

with $e_{ij}(t)$ being the j^{th} entry of $e_i(t)$. The second term on the right-hand-side of (53) can be written as follows

$$\frac{d}{dt} \begin{bmatrix} z_1 & z_1 & z_2 & z_2 & z_3 & z_3 & z_4 & z_4 \end{bmatrix}^T = C_1 J_r u \quad (55)$$

where (14) was utilized, and the auxiliary matrix $C_1(t) \in \mathbb{R}^{8 \times 6}$ is defined as follows

$$C_1 \triangleq \begin{bmatrix} r_{c3}^T & -R_r & S[R_r(x_{p1} - x_r)] \\ r_{c3}^T & -R_r & S[R_r(x_{p1} - x_r)] \\ r_{c3}^T & -R_r & S[R_r(x_{p2} - x_r)] \\ r_{c3}^T & -R_r & S[R_r(x_{p2} - x_r)] \\ r_{c3}^T & -R_r & S[R_r(x_{p3} - x_r)] \\ r_{c3}^T & -R_r & S[R_r(x_{p3} - x_r)] \\ r_{c3}^T & -R_r & S[R_r(x_{p4} - x_r)] \\ r_{c3}^T & -R_r & S[R_r(x_{p4} - x_r)] \end{bmatrix}. \quad (56)$$

The auxiliary signal $\Pi(t)$, introduced in (20), is defined as follows

$$\Pi \triangleq \left(B_1 + \frac{1}{2} E_1 C_1 \right) J_r \quad (57)$$

where (19), (20), (53)-(55) were all utilized. The auxiliary matrix $F_1(t) \in \mathbb{R}^{8 \times 8}$, introduced in (43), is defined as follows

$$F_1 \triangleq \text{diag} \left\{ \frac{1}{W_{21}\Theta_{21}}, \frac{1}{W_{21}\Theta_{21}}, \frac{1}{W_{22}\Theta_{22}}, \frac{1}{W_{22}\Theta_{22}}, \frac{1}{W_{23}\Theta_{23}}, \frac{1}{W_{23}\Theta_{23}}, \frac{1}{W_{24}\Theta_{24}}, \frac{1}{W_{24}\Theta_{24}} \right\}. \quad (58)$$

APPENDIX II PROOF OF THEOREM

Proof: To facilitate the proof, a nonnegative Lyapunov function $V_1(t) \in \mathbb{R}$ is defined as follows

$$V_1 \triangleq \frac{1}{2} e^T Z e \quad (59)$$

where $Z(t)$ was defined in (15). The time derivative of (59) is given as follows

$$\dot{V}_1 = e^T Z \dot{e} + \frac{1}{2} e^T \dot{Z} e. \quad (60)$$

The expression in (60) can be written as follows

$$\dot{V}_1 = -k e^T \hat{\Pi} \hat{\Pi}^T e + e^T W_3 \tilde{\Theta}. \quad (61)$$

where the closed-loop error system given in (28) was utilized.

To facilitate the analysis another nonnegative Lyapunov function, denoted by $V_2(t) \in \mathbb{R}$, is defined as follows

$$V_2 \triangleq \frac{1}{2} \tilde{\Theta}^T \Gamma^{-1} \tilde{\Theta}. \quad (62)$$

After taking the time derivative of (62) and substituting (44) and (48), the following expression is obtained

$$\dot{V}_2 = -\tilde{\Theta}^T \Gamma^{-1} \text{Proj} \{ \alpha \Gamma \bar{W}^T \tilde{p} + \Gamma W_3^T e \} + \tilde{\Theta}^T \bar{W}^T \bar{W} \tilde{\Theta}. \quad (63)$$

After utilizing the property of the projection (see (116) in Appendix VI), $\dot{V}_2(t)$ can be upper bounded as follows

$$\dot{V}_2 \leq -\alpha \tilde{\Theta}^T \bar{W}^T \tilde{p} + \tilde{\Theta}^T \bar{W}^T \bar{W} \tilde{\Theta} - \tilde{\Theta}^T W_3^T e. \quad (64)$$

The expression in (64) can be rewritten as follows

$$\dot{V}_2 \leq -\alpha \tilde{p}^T F_1^{-T} \tilde{p} + \tilde{p}^T F_1^{-T} F_1^{-1} \tilde{p} - \tilde{\Theta}^T W_3^T e \quad (65)$$

where (43) was utilized. The right-hand-side of (65) can be upper bounded

$$\dot{V}_2 \leq -\alpha \tilde{p}^T \tilde{p} + \tilde{p}^T \tilde{p} - \tilde{\Theta}^T W_3^T e \quad (66)$$

where the definition of $F_1(t)$ in (58) is utilized along with (34), (46), and (47). After utilizing the definition of $\alpha(t)$ in (45) the expression in (66) can be written as follows

$$\dot{V}_2 \leq -\tilde{\epsilon} \|\tilde{p}\|^2 - \tilde{\Theta}^T W_3^T e. \quad (67)$$

To prove the theorem, the following nonnegative Lyapunov function, denoted by $V(t) \in \mathbb{R}$ is defined

$$V \triangleq V_1 + V_2 \quad (68)$$

where $V_1(t)$ and $V_2(t)$ were defined in (59) and (62) respectively. The time derivative of (68) can be upper bounded as follows

$$\dot{V} \leq -k e^T \hat{\Pi} \hat{\Pi}^T e - \tilde{\epsilon} \|\tilde{p}\|^2 \quad (69)$$

where (61) and (67) were utilized. From (69), the following inequalities can be written

$$\dot{V} \leq -k e^T \hat{\Pi} \hat{\Pi}^T e \quad (70)$$

$$\dot{V} \leq -\tilde{\epsilon} \|\tilde{p}\|^2. \quad (71)$$

After integrating (70) and (71), following expressions can be obtained

$$k \int_{t_0}^{+\infty} \left\| \hat{\Pi}^T(\tau) e(\tau) \right\|^2 d\tau < V(t_0) - V(+\infty). \quad (72)$$

$$\tilde{\epsilon} \int_{t_0}^{+\infty} \|\tilde{p}(\tau)\|^2 d\tau < V(t_0) - V(+\infty) \quad (73)$$

After utilizing (72), (73) and the fact that $V(t)$ is nonnegative, it can be concluded that $V(t) < V(t_0)$ for $\forall t$. Hence,

$V(t)$ is bounded (i.e., $V(t) \in \mathcal{L}_\infty$). Then, from (68) it can be concluded that $V_1(t), V_2(t) \in \mathcal{L}_\infty$. Since $V(t)$ is bounded then from (72) and (73), it is clear that $\hat{\Pi}^T(t)e(t), \tilde{p}(t) \in \mathcal{L}_2$. Since $z_i(t)$ are bounded for $\forall i = 1, \dots, 4$ then from (15) it follows that $Z(t) \in \mathcal{L}_\infty$. After utilizing the facts that $V_1(t), Z(t) \in \mathcal{L}_\infty$ along with (59), it follows that $e(t) \in \mathcal{L}_\infty$. From the definition of $e(t)$ in (16), it is clear that $e_i(t) \in \mathcal{L}_\infty \forall i = 1, \dots, 4$. After utilizing the fact that the desired image coordinates $p_{di} \forall i = 1, \dots, 4$ are constant along with the fact that $e_i(t) \forall i = 1, \dots, 4$ are bounded, then from (6), it is clear that $p_i(t) \in \mathcal{L}_\infty \forall i = 1, \dots, 4$. Based on Remark 3, it follows that $q(t)$ is bounded. Since $p_i(t) \forall i = 1, \dots, 4$ are bounded then from (9) it is clear that $\bar{A}_{ei}(t) \in \mathcal{L}_\infty \forall i = 1, \dots, 4$. Since $z_i(t)$ are bounded, from (33) it is easy to see that $W_2(t) \in \mathcal{L}_\infty$. After utilizing the facts that $p_i(t), W_2(t) \in \mathcal{L}_\infty$ along with (35), it is clear that $W_1(t) \in \mathcal{L}_\infty$. By using (34) along with (38), it can be proven that $\bar{W}_i \begin{bmatrix} \tilde{\Theta}_{1i}^T & \tilde{\Theta}_{2i}^T \end{bmatrix}^T \in \mathcal{L}_2$. From (34), it is clear that $F_1(t)$ is bounded. After utilizing the above facts along with (43), it can be concluded that $\bar{W}(t)\tilde{\Theta}(t) \in \mathcal{L}_2$. The fact that $V_2(t)$ is bounded can be used along with (62) to show that $\tilde{\Theta}^T(t)\Gamma^{-1}(t)\tilde{\Theta}(t) \in \mathcal{L}_\infty$. Since $\Gamma^{-1}(t)$ is always positive definite (see Remark 6), then from (62), it is clear that $\tilde{\Theta}(t) \in \mathcal{L}_\infty$. From (26), it is easy to see that $\hat{\Theta}(t) \in \mathcal{L}_\infty$. After utilizing the above boundedness statements along with (37), it is clear that $\hat{p}_i(t) \in \mathcal{L}_\infty$, then from (40), it is easy to see that $\tilde{p}_i(t) \in \mathcal{L}_\infty$. The above mentioned boundedness statements can be used to prove that $\bar{W}(t)$ is bounded. After utilizing the above mentioned boundedness statements, Remarks 3 and 4, along with (52), (54), and (56); then from (57), it is clear that $\Pi(t) \in \mathcal{L}_\infty$. Since $\hat{\Pi}(t)$ is a function of $\hat{\Theta}(t)$ and bounded signals, then it is bounded. The above boundedness statements can be utilized along with (27) to show that $u(t) \in \mathcal{L}_\infty$. Then, from (21), it is clear that $W_3(t) \in \mathcal{L}_\infty$. Since the projection algorithm provides bounded outputs then from (44), it can be concluded that $\dot{\hat{\Theta}}(t) \in \mathcal{L}_\infty$, then the time derivative of (26) can be used to show that $\dot{\hat{\Theta}}(t) \in \mathcal{L}_\infty$. After utilizing the above boundedness statements along with (13), it is clear that $\dot{e}_i(t) \in \mathcal{L}_\infty \forall i = 1, \dots, 4$. From (7), it is clear that $\dot{p}_i(t) \in \mathcal{L}_\infty$. Since $\dot{p}_i(t) \forall i = 1, \dots, 4$ are bounded then, from the time derivative of (9), it is clear that $\frac{d}{dt}\bar{A}_{ei}(t) \in \mathcal{L}_\infty \forall i = 1, \dots, 4$. After utilizing the above boundedness statements, along with the fact that it is a function of $\dot{\hat{\Theta}}(t)$ and bounded signals, it is easy to see that $\frac{d}{dt}\hat{\Pi}(t) \in \mathcal{L}_\infty$. Now, it follows that $\frac{d}{dt}(\hat{\Pi}^T(t)e(t)) \in \mathcal{L}_\infty$. Since $\hat{\Pi}^T(t)e(t) \in \mathcal{L}_2 \cap \mathcal{L}_\infty$, it can be concluded that [27]

$$\left\| \hat{\Pi}^T(t)e(t) \right\| \rightarrow 0 \text{ as } t \rightarrow +\infty. \quad (74)$$

After utilizing Remarks 3 and 4 along with (14), it is clear that $\dot{z}_i(t) \in \mathcal{L}_\infty \forall i = 1, \dots, 4$; hence, from the time derivative of (33), it is clear that $\dot{W}_2(t) \in \mathcal{L}_\infty$. After utilizing the above boundedness statements along with the time derivatives of (32) and (36), it can be proven that $\dot{W}_1(t), \dot{p}_i(t) \in \mathcal{L}_\infty$, hence proving that $\dot{\bar{W}}(t) \in \mathcal{L}_\infty$. The previously

mentioned boundedness statements can be utilized to prove that $\frac{d}{dt}(\bar{W}(t)\tilde{\Theta}(t)) \in \mathcal{L}_\infty$. Since $\bar{W}(t)\tilde{\Theta}(t) \in \mathcal{L}_2 \cap \mathcal{L}_\infty$, it can be concluded that [27]

$$\left\| \bar{W}(t)\tilde{\Theta}(t) \right\| \rightarrow 0 \text{ as } t \rightarrow +\infty. \quad (75)$$

As shown in Appendices III and IV, if the signals $\hat{\Pi}(t)$ and $\bar{W}(t)$ satisfy the persistent excitation (PE) conditions given in (50), (51), then from (74) and (75) it can further be concluded that

$$\|e(t)\| \rightarrow 0 \text{ as } t \rightarrow +\infty \quad (76)$$

$$\left\| \tilde{\Theta}(t) \right\| \rightarrow 0 \text{ as } t \rightarrow +\infty. \quad (77)$$

APPENDIX III PE PROOF FOR $e(t)$

An auxiliary function $\Omega_1(t_0, t) \in \mathbb{R}^{8 \times 8}$ is defined as follows

$$\Omega_1 \triangleq \int_{t_0}^t \hat{\Pi}(\tau)\hat{\Pi}^T(\tau)d\tau. \quad (78)$$

To facilitate the proof the following expression is considered

$$\begin{aligned} \frac{d}{d\tau} \{e^T(\tau)\Omega_1(t_0, \tau)e(\tau)\} &= \dot{e}^T(\tau)\Omega_1(t_0, \tau)e(\tau) \\ &+ e^T(\tau)\frac{d}{d\tau}\{\Omega_1(t_0, \tau)\}e(\tau) + e^T(\tau)\Omega_1(t_0, \tau)\dot{e}(\tau). \end{aligned} \quad (79)$$

From (79), the following expression can be obtained after integrating from t_0 to t and rearranging the terms

$$\begin{aligned} \int_{t_0}^t e^T(\tau)\Omega_1(t_0, \tau)\dot{e}(\tau)d\tau &= e^T(t)\Omega_1(t_0, t)e(t) \\ -e^T(t_0)\Omega_1(t_0, t_0)e(t_0) &- \int_{t_0}^t \dot{e}^T(\tau)\Omega_1(t_0, \tau)e(\tau)d\tau \\ - \int_{t_0}^t e^T(\tau)\frac{d}{d\tau}\{\Omega_1(t_0, \tau)\}e(\tau)d\tau. \end{aligned} \quad (80)$$

After utilizing the following facts

$$\begin{aligned} \Omega_1(t_0, t_0) &= 0_{8 \times 8} \\ \Omega_1^T(t_0, \tau) &= \Omega_1(t_0, \tau) \\ \frac{d}{d\tau}\{\Omega_1(t_0, \tau)\} &= \hat{\Pi}(\tau)\hat{\Pi}^T(\tau), \end{aligned} \quad (81)$$

the expression in (80) can be rearranged as follows

$$\begin{aligned} &e^T(t)\Omega_1(t_0, t)e(t) \\ &= 2 \int_{t_0}^t e^T(\tau)\Omega_1(t_0, \tau)\dot{e}(\tau)d\tau \\ &+ \int_{t_0}^t e^T(\tau)\hat{\Pi}(\tau)\hat{\Pi}^T(\tau)e(\tau)d\tau \end{aligned} \quad (82)$$

where $0_{8 \times 8} \in \mathbb{R}^{8 \times 8}$ is a matrix of zeros. To further facilitate the proof, the following lemma is stated [28]:

Lemma 1: Let $f(t)$ be a uniformly continuous function [27]. Then,

$$\lim_{t \rightarrow +\infty} f(t) = 0 \Leftrightarrow \lim_{t \rightarrow +\infty} \int_t^{t+t'} f(\tau) d\tau = 0 \quad (83)$$

for any positive constant $t' \in \mathbb{R}$.

To utilize Lemma 1, a change of variables is applied to (82) by substituting t with $t_0 + T$, where $T \in \mathbb{R}$ is a positive constant. The following expression is obtained after applying a limit operation to the resulting equation

$$\begin{aligned} & \lim_{t_0 \rightarrow +\infty} e^T(t_0 + T) \Omega_1(t_0, t_0 + T) e(t_0 + T) \\ &= 2 \lim_{t_0 \rightarrow +\infty} \int_{t_0}^{t_0+T} e^T(\tau) \Omega_1(t_0, \tau) \dot{e}(\tau) d\tau \\ &+ \lim_{t_0 \rightarrow +\infty} \int_{t_0}^{t_0+T} e^T(\tau) \hat{\Pi}(\tau) \hat{\Pi}^T(\tau) e(\tau) d\tau. \end{aligned} \quad (84)$$

Remark 7: The right-hand-side of (18) can be written as follows

$$Z\dot{e} = -kB_1 J_r \hat{\Pi}^T e \quad (85)$$

where (27) was utilized. After utilizing (74), it is easy to see that the right-hand-side of (85) goes to zero. After utilizing this fact along with the fact that $Z(t)$ is positive definite, then it is clear that

$$\|\dot{e}(t)\| \rightarrow 0 \text{ as } t \rightarrow +\infty. \quad (86)$$

After utilizing (50), (86), Lemma 1, and the fact that $e(t)$ is bounded, then it is clear that the first term at the right-hand-side of (84) is equal to zero. After utilizing (74), Lemma 1, and the facts that $\hat{\Pi}(t)$, $e(t)$ are bounded, then it is clear that the second term at the right-hand-side of (84) is equal to zero. Thus the following expression can be obtained based on (84)

$$\lim_{t_0 \rightarrow +\infty} e^T(t_0 + T) \Omega_1(t_0, t_0 + T) e(t_0 + T) = 0. \quad (87)$$

After utilizing the fact that $\gamma_1 I_8 \leq \Omega_1(t_0, t_0 + T)$ it is clear that

$$\|e(t)\| \rightarrow 0 \text{ as } t \rightarrow +\infty. \quad (88)$$

APPENDIX IV PE PROOF FOR $\tilde{\Theta}(t)$

An auxiliary function $\Omega_2(t_0, t) \in \mathbb{R}^{p \times p}$ is defined as follows

$$\Omega_2 \triangleq \int_{t_0}^t \bar{W}^T(\tau) \bar{W}(\tau) d\tau. \quad (89)$$

To facilitate the proof the following expression is considered

$$\begin{aligned} & \frac{d}{d\tau} \left\{ \tilde{\Theta}^T(\tau) \Omega_2(t_0, \tau) \tilde{\Theta}(\tau) \right\} \\ &= \dot{\tilde{\Theta}}^T(\tau) \Omega_2(t_0, \tau) \tilde{\Theta}(\tau) \\ &+ \tilde{\Theta}^T(\tau) \frac{d}{d\tau} \{ \Omega_2(t_0, \tau) \} \tilde{\Theta}(\tau) \\ &+ \tilde{\Theta}^T(\tau) \Omega_2(t_0, \tau) \dot{\tilde{\Theta}}(\tau). \end{aligned} \quad (90)$$

From (90), the following expression can be obtained after integrating from t_0 to t and rearranging the terms

$$\begin{aligned} & \int_{t_0}^t \tilde{\Theta}^T(\tau) \Omega_2(t_0, \tau) \dot{\tilde{\Theta}}(\tau) d\tau \\ &= \tilde{\Theta}^T(t) \Omega_2(t_0, t) \tilde{\Theta}(t) - \tilde{\Theta}^T(t_0) \Omega_2(t_0, t_0) \tilde{\Theta}(t_0) \\ &\quad - \int_{t_0}^t \dot{\tilde{\Theta}}^T(\tau) \Omega_2(t_0, \tau) \tilde{\Theta}(\tau) d\tau \\ &\quad - \int_{t_0}^t \tilde{\Theta}^T(\tau) \frac{d}{d\tau} \{ \Omega_2(t_0, \tau) \} \tilde{\Theta}(\tau) d\tau. \end{aligned} \quad (91)$$

After utilizing the following facts

$$\Omega_2(t_0, t_0) = 0_{p \times p} \quad (92)$$

$$\Omega_2^T(t_0, \tau) = \Omega_2(t_0, \tau)$$

$$\frac{d}{d\tau} \{ \Omega_2(t_0, \tau) \} = \bar{W}^T(\tau) \bar{W}(\tau),$$

the expression in (91) can be rearranged as follows

$$\begin{aligned} & \tilde{\Theta}^T(t) \Omega_2(t_0, t) \tilde{\Theta}(t) \\ &= 2 \int_{t_0}^t \tilde{\Theta}^T(\tau) \Omega_2(t_0, \tau) \dot{\tilde{\Theta}}(\tau) d\tau \\ &+ \int_{t_0}^t \tilde{\Theta}^T(\tau) \bar{W}^T(\tau) \bar{W}(\tau) \tilde{\Theta}(\tau) d\tau \end{aligned} \quad (93)$$

where $0_{p \times p} \in \mathbb{R}^{p \times p}$ is a matrix of zeros. A change of variables is applied to (93) by substituting t with $t_0 + T$. The following equation is obtained after applying a limit operation to the resulting equation

$$\begin{aligned} & \lim_{t_0 \rightarrow +\infty} \tilde{\Theta}^T(t_0 + T) \Omega_2(t_0, t_0 + T) \tilde{\Theta}(t_0 + T) \\ &= 2 \lim_{t_0 \rightarrow +\infty} \int_{t_0}^{t_0+T} \tilde{\Theta}^T(\tau) \Omega_2(t_0, \tau) \dot{\tilde{\Theta}}(\tau) d\tau \\ &+ \lim_{t_0 \rightarrow +\infty} \int_{t_0}^{t_0+T} \tilde{\Theta}^T(\tau) \bar{W}^T(\tau) \bar{W}(\tau) \tilde{\Theta}(\tau) d\tau. \end{aligned} \quad (94)$$

Remark 8: The right-hand-side of (44) can be written as follows

$$\dot{\Theta} = \text{Proj} \left\{ \alpha \Gamma \bar{W}^T \frac{1}{W_2 \Theta_2} \bar{W} \tilde{\Theta} + \Gamma W_3^T e \right\} \quad (95)$$

where (38) was utilized. From (75), it is clear that the first term inside the bracket on the right-hand-side of (95) goes to zero, and from (88) the second term inside the bracket goes to zero. So, both $\dot{\Theta}$ and $\dot{\tilde{\Theta}}(t)$ go to zero as $t \rightarrow +\infty$.

After utilizing (51), (95), Lemma 1, and the fact that $\tilde{\Theta}(t)$ is bounded, it is clear that the first term at the right-hand-side of (94) is equal to zero. After utilizing (75), Lemma 1, and the facts that $\bar{W}(\tau)$, $\tilde{\Theta}(\tau)$ are bounded, it is clear that the second term at the right-hand-side of (94) is equal to zero. Thus the following expression can be obtained based on (94)

$$\lim_{t_0 \rightarrow +\infty} \tilde{\Theta}^T(t_0 + T) \Omega_2(t_0, t_0 + T) \tilde{\Theta}(t_0 + T) = 0. \quad (96)$$

After utilizing the fact that $\gamma_3 I_p \leq \Omega_2(t_0, t_0 + T)$ it is clear that

$$\|\tilde{\Theta}(t)\| \rightarrow 0 \text{ as } t \rightarrow +\infty. \quad (97)$$

APPENDIX V EXTENSION TO FIXED-CAMERA CONFIGURATION

In this section, an extension to fixed-camera configuration is presented. The analysis for the fixed-camera configuration varies from the camera-in-hand configuration only for the open-loop error system development. The rest of the analysis are same for both configurations. The error system development for the fixed-camera case is presented below.

In order to develop a geometric relationship between fixed-camera and moving object, an orthogonal coordinate frame, denoted by \mathcal{F} , attached to the object, an inertial coordinate frame, denoted by \mathcal{I} , whose origin coincides with the optical center of the fixed-camera, and an inertial coordinate frame, denoted by \mathcal{W} , attached to the base frame of the robot manipulator are defined (see Figure 2). Let the 3D coordinates of the i^{th} feature point on the object be denoted by the constant $s_i \in \mathbb{R}^3$ relative to the object reference frame \mathcal{F} , and $\bar{m}_i(t) \in \mathbb{R}^3$ relative to the inertial coordinate frame \mathcal{I} , which is defined in (1).

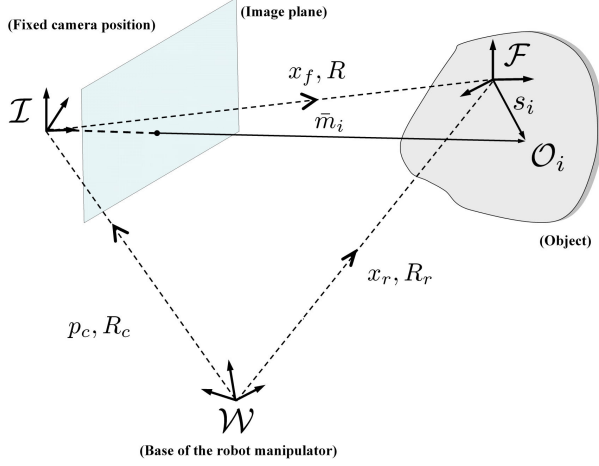


Fig. 2. Geometric relationships between the fixed-camera, robot manipulator and the object attached to its end-effector.

The image error for the i^{th} feature point, denoted by $e_i(t) \in \mathbb{R}^2$ is defined in (6). To facilitate the error system development the dynamics of the image error is found as follows

$$\dot{e}_i = \frac{1}{z_i} \bar{A}_{ei} R_c \begin{bmatrix} R_r & R_r S(s_i) \end{bmatrix} J_r u. \quad (98)$$

In (98), $\bar{A}_{ei}(t) \in \mathbb{R}^{2 \times 3}$ is a function of camera intrinsic calibration parameters and image coordinates of the i^{th} feature point, defined in (9), $R_c \in SO(3)$ is the camera extrinsic calibration matrix, $R_r(t) \in SO(3)$ is the orientation matrix of the end-effector of the robot manipulator, $J_r(q) \in \mathbb{R}^{6 \times 6}$ is the Jacobian matrix of the robot manipulator, and $u(t) \in \mathbb{R}^6$ represents the kinematic control input. It should be noted that Remarks 2, 3, and 4 are satisfied for the fixed-camera configuration.

Remark 9: In the subsequent analysis, it is assumed that $s_i \in \mathbb{R}^3$ are known (see [29] for the precedence of this kind of assumption).

After utilizing (1) and (98), the dynamics of $z_i(t)$ is obtained as follows

$$\dot{z}_i = r_{c3}^T \begin{bmatrix} R_r & R_r S(s_i) \end{bmatrix} J_r u \quad (99)$$

where $r_{c3}^T \in \mathbb{R}^{1 \times 3}$ is the third row vector of extrinsic camera calibration matrix.

To facilitate the subsequent analysis a diagonal matrix, denoted by $Z(t) \in \mathbb{R}^{8 \times 8}$ with its entries being $z_i(t) \forall i = 1, \dots, 4$, and a combined error signal $e(t) \in \mathbb{R}^8$ are defined as in (15) and (16). After utilizing (15), (16), and (98), the following expression can be obtained

$$Z \dot{e} = B_1 J_r u \quad (100)$$

where auxiliary signal $B_1(t) \in \mathbb{R}^{8 \times 6}$ is defined as follows

$$B_1 \triangleq \begin{bmatrix} \bar{A}_{e1} R_c \begin{bmatrix} R_r & R_r S(s_1) \end{bmatrix} \\ \bar{A}_{e2} R_c \begin{bmatrix} R_r & R_r S(s_2) \end{bmatrix} \\ \bar{A}_{e3} R_c \begin{bmatrix} R_r & R_r S(s_3) \end{bmatrix} \\ \bar{A}_{e4} R_c \begin{bmatrix} R_r & R_r S(s_4) \end{bmatrix} \end{bmatrix}. \quad (101)$$

After utilizing (16) and the time derivative of (15), $\dot{Z}(t)e(t)$ can be written as follows

$$\dot{Z}e = E_1 \frac{d}{dt} \begin{bmatrix} z_1 & z_1 & z_2 & z_2 & z_3 & z_3 & z_4 & z_4 \end{bmatrix}^T \quad (102)$$

where diagonal matrix $E_1(t) \in \mathbb{R}^{8 \times 8}$ is defined as follows

$$E_1 \triangleq \text{diag} \{e_{11}, e_{12}, e_{21}, e_{22}, e_{31}, e_{32}, e_{41}, e_{42}\} \quad (103)$$

with $e_{ij}(t)$ being the j^{th} entry of $e_i(t)$. The second term on the right-hand-side of (102) can be written as follows

$$\frac{d}{dt} \begin{bmatrix} z_1 & z_1 & z_2 & z_2 & z_3 & z_3 & z_4 & z_4 \end{bmatrix}^T = C_1 J_r u \quad (104)$$

where auxiliary signal $C_1(t) \in \mathbb{R}^{8 \times 6}$ is defined as follows

$$C_1 \triangleq \begin{bmatrix} r_{c3}^T \begin{bmatrix} R_r & R_r S(s_1) \end{bmatrix} \\ r_{c3}^T \begin{bmatrix} R_r & R_r S(s_1) \end{bmatrix} \\ r_{c3}^T \begin{bmatrix} R_r & R_r S(s_2) \end{bmatrix} \\ r_{c3}^T \begin{bmatrix} R_r & R_r S(s_2) \end{bmatrix} \\ r_{c3}^T \begin{bmatrix} R_r & R_r S(s_3) \end{bmatrix} \\ r_{c3}^T \begin{bmatrix} R_r & R_r S(s_3) \end{bmatrix} \\ r_{c3}^T \begin{bmatrix} R_r & R_r S(s_4) \end{bmatrix} \\ r_{c3}^T \begin{bmatrix} R_r & R_r S(s_4) \end{bmatrix} \end{bmatrix} \quad (105)$$

where (99) was utilized.

A prediction error formulation for the unknown parameters will be introduced. From Figure 2, $\bar{m}_i(t)$ can be written as follows⁵

$$\bar{m}_i = R_c x_r + R_c R_r s_i + p_c \quad (106)$$

where $p_c \in \mathbb{R}^3$ is the position of the origin of frame \mathcal{I} with respect to frame \mathcal{W} expressed in frame \mathcal{W} . After utilizing

⁵For the derivation of the expression for \bar{m}_i the reader is referred to Appendix VII.

(1), (2), and (4), the pixel coordinates for the i^{th} feature point can be written as follows

$$p_i = \frac{1}{z_i} \bar{A} [R_c x_r + R_c R_r s_i + p_c] \quad (107)$$

where the corresponding depth can be written as follows

$$z_i = r_{c3}^T x_r + r_{c3}^T R_r s_i + p_{c3} \quad (108)$$

where $r_3^T(t) \in \mathbb{R}^3$ is the last row of $R(t)$. It should be noted that, in (107) and (108), \bar{A} , R_c , s_i , p_c are unknown constant parameters, and $x_r(t)$, $R_r(t)$ are measurable signals (see Remark 2). The rest of the prediction error formulation is same as the camera-in-hand configuration.

APPENDIX VI PROJECTION ALGORITHM

The positiveness of the term $W_2(t) \hat{\Theta}_2(t)$ is ensured by a projection operator on $\hat{\Theta}(t)$ [24]. To facilitate the subsequent development, an auxiliary scalar function is defined as follows

$$\mathcal{P}(\hat{\Theta}) \triangleq \varepsilon - W_2 \hat{\Theta}_2 \quad (109)$$

where its gradient is computed as follows

$$\nabla_{\hat{\Theta}} \mathcal{P}(\hat{\Theta}) = \begin{bmatrix} 0_{1 \times r_1} & -W_2 \end{bmatrix} \quad (110)$$

where ε being an arbitrarily small positive constant and $0_{1 \times r_1} \in \mathbb{R}^{1 \times r_1}$ being a vector of zeros. Two convex sets based on the function $\mathcal{P}(\hat{\Theta})$ are defined as follows

$$\mathcal{R} \triangleq \left\{ \hat{\Theta} \in \mathbb{R}^p : \mathcal{P}(\hat{\Theta}) \leq 0 \right\} \quad (111)$$

$$\mathcal{R}_\delta \triangleq \left\{ \hat{\Theta} \in \mathbb{R}^p : \mathcal{P}(\hat{\Theta}) \leq \delta \right\} \quad (112)$$

where $\delta \in \mathbb{R}$ is a positive constant that is very close to zero.

Let the boundary and the interior of set \mathcal{R} be defined by $\partial \mathcal{R}$ and $\overset{\circ}{\mathcal{R}}$, respectively. Based on these definitions, the projection of $\tau(t)$ is defined as follows

$$\text{Proj}\{\tau\} \triangleq \begin{cases} \tau & \hat{\Theta} \in \overset{\circ}{\mathcal{R}} \text{ or } \nabla_{\hat{\Theta}} \mathcal{P}^T \tau \leq 0 \\ P_\tau & \hat{\Theta} \in \mathcal{R}_\delta \setminus \overset{\circ}{\mathcal{R}} \text{ and } \nabla_{\hat{\Theta}} \mathcal{P}^T \tau > 0 \end{cases} \quad (113)$$

where $P_\tau(t) \in \mathbb{R}^p$ is defined as follows

$$P_\tau = \left(I - c(\hat{\Theta}) \Gamma \frac{\nabla_{\hat{\Theta}} \mathcal{P} \nabla_{\hat{\Theta}} \mathcal{P}^T}{\nabla_{\hat{\Theta}} \mathcal{P}^T \Gamma \nabla_{\hat{\Theta}} \mathcal{P}} \right) \tau \quad (114)$$

where the auxiliary scalar function $c(\hat{\Theta})$ is defined as follows

$$c(\hat{\Theta}) \triangleq \min \left\{ 1, \frac{\mathcal{P}(\hat{\Theta})}{\delta} \right\}. \quad (115)$$

It is helpful to note that $c(\partial \mathcal{R}) = 0$ and $c(\partial \mathcal{R}_\delta) = 1$. The suggested projection operator satisfies the following property (reader is referred to [24] for the proof)

$$-\tilde{\Theta}^T \Gamma^{-1} \text{Proj}\{\tau\} \leq -\tilde{\Theta}^T \Gamma^{-1} \tau, \quad \forall \hat{\Theta} \in \mathcal{R}_\delta, \quad \Theta \in \mathcal{R}. \quad (116)$$

APPENDIX VII DERIVATION OF $\bar{m}_i(t)$

A. Camera-In-Hand Configuration

In Figure 1, let the vector representing the distance between the origin of \mathcal{E} and \mathcal{O}_i be denoted as $\bar{x}_i(t) \in \mathbb{R}^3$. From the triangle formed by \mathcal{O}_i and the origins of \mathcal{F} and \mathcal{E} , it is easy to see that

$$\bar{m}_i = R_c \bar{x}_i + p_c. \quad (117)$$

Similarly, from the triangle formed by \mathcal{O}_i and the origins of \mathcal{W} and \mathcal{E} , the following can be obtained

$$\bar{x}_{pi} = R_r \bar{x}_i + x_r. \quad (118)$$

After solving (118) for $\bar{x}_i(t)$ and substituting the resulting expression into (117), we obtain

$$\bar{m}_i = R_c [R_r^T (x_{pi} - x_r) + p_c]. \quad (119)$$

B. Fixed-Camera Configuration

In Figure 2, from the triangle formed by \mathcal{O}_i and the origins of \mathcal{F} and \mathcal{I} , it is easy to see that

$$\bar{m}_i = R_c R_r s_i + x_f. \quad (120)$$

Similarly, from the triangle formed by the origins of \mathcal{W} , \mathcal{I} and \mathcal{F} , the following can be obtained

$$\bar{x}_f = R_c \bar{x}_r + p_c. \quad (121)$$

After substituting $\bar{x}_i(t)$ found in (121) into (120), we obtain

$$\bar{m}_i = R_c x_r + R_c R_r s_i + p_c. \quad (122)$$